

# Crossover Time in Relative Fluctuations Characterizes the Longest Relaxation Time of Entangled Polymers

Takashi Uneyama

*JST-CREST, Institute for Chemical Research, Kyoto University, Gokasho, Uji 611-0011, Japan and  
School of Natural System, College of Science and Engineering,  
Kanazawa University, Kakuma, Kanazawa 920-1192, Japan*

Takuma Akimoto

*Department of Mechanical Engineering, Keio University, Yokohama 223-8522, Japan*

Tomoshige Miyaguchi

*Department of Mathematics Education, Naruto University of Education, Tokushima 772-8502, Japan*

(Dated: November 17, 2018)

In entangled polymer systems, there are several characteristic time scales, such as the entanglement time and the disengagement time. In molecular simulations, the longest relaxation time (the disengagement time) can be determined by the mean square displacement (MSD) of a segment or by the shear relaxation modulus. Here, we propose the relative fluctuation analysis method, which is originally developed for characterizing large fluctuations, to determine the longest relaxation time from the center of mass trajectories of polymer chains (the time-averaged MSDs). Applying the method to simulation data of entangled polymers (by the slip-spring model and the simple reptation model), we provide a clear evidence that the longest relaxation time is estimated as the crossover time in the relative fluctuations.

## I. INTRODUCTION

Polymer melts and solutions exhibit interesting dynamical behavior. In particular, if the degree of polymerization is large, characteristic dynamical behavior due to the entanglement effect can be observed[1]. For example, viscoelasticity with a very long relaxation time (which strongly depends on the molecular weight) and anomalous diffusion of a segment occur as a result of the entanglement effect. Dynamics of entangled polymers have been studied extensively by various methods[1–3], including theoretical modeling and simulations.

There are several characteristic time scales in entangled polymer systems, such as the entanglement time  $\tau_e$ , the Rouse time  $\tau_R$ , and the disengagement time (the longest relaxation time)  $\tau_d$ . In each characteristic time scale, mean square displacements (MSDs) show different scalings. For example, the Doi-Edwards tube model gives the following time dependence of the MSD of a single segment[1]:

$$\langle [\mathbf{r}_i(t) - \mathbf{r}_i(0)]^2 \rangle \propto \begin{cases} t^{1/2} & (t \lesssim \tau_e) \\ t^{1/4} & (\tau_e \lesssim t \lesssim \tau_R) \\ t^{1/2} & (\tau_R \lesssim t \lesssim \tau_d) \\ t & (\tau_d \lesssim t), \end{cases} \quad (1)$$

where  $\mathbf{r}_i(t)$  is the position of the  $i$ -th segment at time  $t$  and  $\langle \dots \rangle$  represents the ensemble average. Anomalous diffusion of a single segment in the Doi-Edwards tube model originates from the following two mechanisms. One is a dynamical property of a single Rouse chain. The MSD of a segment of a Rouse chain shows subdiffusive behavior,  $\langle [\mathbf{r}_i(t) - \mathbf{r}_i(0)]^2 \rangle \propto t^{1/2}$ , at the short time scale ( $t \lesssim \tau_R$ )[1]. The other is a constraint by a tube (which is formed by surrounding chains). Namely, each segment can move only along the tube, which has a fractal geometry similar to a random walk trajectory, thereby causing a subdiffusive transport characterized by the exponent 1/2 for  $\tau_e \lesssim t \lesssim \tau_d$ . The subdiffusive exponent 1/4 for  $\tau_e \lesssim t \lesssim \tau_R$  results from the combination of these two mechanisms. Thus, using the MSD of a single segment, one can estimate  $\tau_e$ ,  $\tau_R$  and  $\tau_d$ [4–6].

It should be noticed that numerical prefactors in Eq. (1) (which are not explicitly shown) depend on the index  $i$  if the target segment is close to chain ends[6]. (And if the strong  $i$ -dependence is observed, validity of Eq. (1) is no longer guaranteed.) Although this does not cause serious problems for relatively fine-scale models (such as the Kremer-Grest model[4–6]), it may be crucial for highly coarse-grained models (such as the RaPiD (responsive particle dynamics) model[7, 8]). In some coarse-grained models, resolutions of the models are not sufficient to resolve the MSDs of segments. Therefore, for such coarse-grained models, it is physically reasonable to employ the MSD of the center of mass (CM) of a chain, instead of that of a single segment. In contrast to the MSD of a single segment, the

MSD of the CM is given by

$$\langle [\mathbf{r}_{\text{CM}}(t) - \mathbf{r}_{\text{CM}}(0)]^2 \rangle \propto \begin{cases} t & (t \lesssim \tau_e) \\ t^{1/2} & (\tau_e \lesssim t \lesssim \tau_R) \\ t & (\tau_R \lesssim t), \end{cases} \quad (2)$$

where  $\mathbf{r}_{\text{CM}}(t)$  is the position of the CM. We note that the scaling exponent in the MSD of the CM does not change around  $t \approx \tau_d$ . Roughly speaking, this is because the constraint by a tube apparently disappears by taking the average with respect to all segments. It seems to be difficult to extract an information of  $\tau_d$  from the MSD of the CM straightforwardly.

For highly coarse-grained models, thus, usually other physical quantities such as the shear relaxation modulus and the end-to-end vector relaxation function have been employed to determine the long time relaxation behavior. However, it is not always easy to determine the long time relaxation behavior accurately. For example, to obtain the accurate shear relaxation modulus data, we need to compute the autocorrelation functions of stress tensors for large number of statistically independent samples. Such calculation becomes demanding for interacting many chain models. The end-to-end vector relaxation function can be computed more accurately than the relaxation modulus, but some highly coarse-grained models such as the RaPiD model do not provide the information of end-to-end vectors. Therefore, alternative methods to determine the long time behavior will be useful for some simulation models, and thus are worth developing. A simple but fascinating idea is to utilize some tools or methods developed in the fields other than polymer physics to analyze simulation data of entangled polymers.

In this work, we employ a method which is originally developed in Lévy statistics[9], to analyze the long time relaxation behavior of entangled polymers. Recently, various theoretical tools have been developed for the continuous time random walk (CTRW) model[10], which is a typical trap model. An interesting recent finding is that the distribution of the time-average MSD (TAMSD) can be utilized to characterize some dynamical properties[11–16]. The TAMSD for a position  $\mathbf{r}$  is defined as

$$\overline{\delta^2(\Delta; t)} \equiv \frac{1}{t - \Delta} \int_0^{t-\Delta} dt' [\mathbf{r}(t' + \Delta) - \mathbf{r}(t')]^2, \quad (3)$$

with  $\Delta$  and  $t$  being the time difference and the observation time. The relative fluctuation (RF) of the TAMSD

$$R(t; \Delta) \equiv \frac{\langle |\overline{\delta^2(\Delta; t)} - \langle \overline{\delta^2(\Delta; t)} \rangle| \rangle}{\langle \overline{\delta^2(\Delta; t)} \rangle}, \quad (4)$$

is useful for characterizing non-Gaussian fluctuations and ergodicity breaking in diffusion processes[11, 13–15]. For the CTRW trajectories, by analyzing the  $t$ -dependence of the RF, we can determine some important information of the trapping-time distribution, such as the power-law exponent and relaxation time[13, 15].

Although the CTRW is not equivalent to models for entangled polymers, the RFs in polymer systems may also characterize some long time relaxation behavior. If the RF analysis (RFA) works well for entangled polymers, it will serve as a new and complementary tool to study the long time relaxation behavior. As far as the authors know, such an analysis has never been performed for entangled polymer systems. In this work we perform the RFA for the CM trajectory data of entangled polymer models and show that the information of the long time relaxation behavior (such as the longest relaxation time  $\tau_d$ ) can be observed. Therefore the RFA can be utilized as a new and complementary method.

## II. SIMULATION RESULTS

In this section, we perform simulations for entangled polymers and analyze MSDs of CMs. So far, various simulation models have been proposed and utilized to study entangled polymers[4, 7, 8, 17–22]. In this work, we employ two simple models among them. One is the slip-spring model[21, 22] and the other is the simple Doi-Edwards type reptation model[23]. We calculate the RFs of the TAMSDs, Eq. (4), for the CM trajectories ( $\mathbf{r}_{\text{CM}}(t)$ ), and show that the RFs show clear crossovers around  $t \simeq \tau_d$ .

### A. Slip-Spring Model

First we perform simulations of the slip-spring model[21, 22]. The slip-spring model is a variant of slip-link models[17–20], which reproduce diffusive and rheological properties well. In the slip-spring model, a polymer chain is

described as an ideal chain and the entanglements are mimicked by so-called slip-springs. One end of a slip-spring is anchored in space while another end can slip along the chain. Moreover, slip-springs are dynamically reconstructed at chain ends. This model can reasonably reproduce linear and nonlinear rheological properties, while it lacks some mechanisms such as the constraint release (CR) or the convective constraint release (CCR)[2, 3]. We perform simulations for different numbers of beads (polymerization indices)  $N$ . Other parameters are set to be the standard values; the average number of segments between slip-springs  $N_0 = 4$ , the slip-spring strength  $N_s = 0.5$ , the friction coefficient of a slip-spring  $\zeta_s/\zeta = 0.1$  (with  $\zeta$  being the friction coefficient of a segment). As elementary length and time scales of this model, we use the segment size  $b$  and the characteristic time of a segment  $\tau_0 \equiv \zeta b^2/k_B T$ . ( $k_B$  and  $T$  are the Boltzmann constant and the temperature, respectively.) For each  $N$  value, simulations are performed for 1024 polymer chains sampled from an equilibrium distribution. (Details of simulation model and algorithm used in this work are described in Ref.[22])

Figure 1 shows the ensemble-averaged MSDs (EAMSDs) of CMs for  $N = 10, 20, 40, 80$ , and 160. (The CM is determined as the average position of the beads which compose a polymer chain.) For large  $N$  cases, the  $t$  dependence of the MSDs is well described by Eq. (2). Thus information of two characteristic times,  $\tau_e$  and  $\tau_R$ , can be obtained. However, as we mentioned in Section I, we cannot obtain any information about  $\tau_d$  from the EAMSDs for CMs. Here we perform the RFA of the TAMSDs for CMs. As will be shown in Appendix A, it is difficult to obtain the RF accurately if  $\Delta$  is too small. Also, if  $\Delta$  is too large, the RF shows only Gaussian fluctuation. Therefore, the time difference  $\Delta$  should be chosen to be some moderate values. Here, we employ  $\Delta/\tau_0 = 10$  for the current slip-spring simulations.

Figure 2 shows the RF for different  $N$ . For large  $N$  cases ( $N \gtrsim 40$ ), the RF is fitted well by the following form except for a very short time region:

$$R(t; \Delta) \propto \begin{cases} t^{-\alpha} & (t \lesssim \tau_c) \\ t^{-0.5} & (t \gtrsim \tau_c) \end{cases}, \quad (5)$$

where  $\alpha$  is a power-law exponent ( $0 < \alpha < 0.5$ ) and  $\tau_c$  is the crossover time. The crossover time,  $\tau_c$ , is much longer than the crossover time for the EAMSD and strongly depends on  $N$ . We cannot determine the crossover time accurately for small  $N$  ( $N \lesssim 20$ , Fig. 2(a)). For  $N \gtrsim 40$  (Fig. 2(b)), we can determine the crossover time from the RF data easily. The crossover time  $\tau_c$  strongly depends on  $N$ . (The power-law exponent  $\alpha$  also depends on  $N$ . Fitting gives  $\alpha = 0.31, 0.24$  and  $0.19$  for  $N = 40, 80$  and  $160$ , respectively. We will discuss this in Section III.) Such behavior of  $\tau_c$  seems to be consistent with the behavior of the longest relaxation time  $\tau_d$  determined from the shear relaxation modulus[22]. Actually, the  $N$  dependence of  $\tau_c$  obtained from the RFA is quite similar to that of  $\tau_d$  (see Fig. 3). For  $N \gtrsim 40$ ,  $\tau_d$  and  $\tau_c$  show the similar power-law type  $N$  dependencies ( $\tau_d \propto N^{3.48}$  and  $\tau_c \propto N^{3.51}$ ).

For  $N \lesssim 20$ , the  $N$  dependence of  $\tau_d$  is close to one of unentangled polymers ( $\tau_d \propto N^2$ ) and in this region  $\tau_c$  is not determined accurately (see Fig. 2(a)). Possibly, this implies that we cannot extract the information about the long time relaxation behavior from the RFA if  $\tau_d$  is comparable to or less than  $\Delta$ . Similar trend is found in Appendix A. Although behavior of the RF of the TAMSDs depends on parameters such as  $N$  and  $\Delta$ , we have qualitatively the same result for other cases as long as  $N$  is sufficiently large. Thus, in the slip-spring model, we conclude that  $\tau_c$  is essentially the same as  $\tau_d$  apart from the numerical constant.

## B. Discrete Reptation Model

To confirm whether the relation between the cutoff time and the longest relaxation time is a general feature in entangled polymer systems, second we perform simulations of the simple Doi-Edwards type reptation model. This model is one of the simplest models for entangled polymers, yet describes some essential features of entangled polymer dynamics qualitatively. The details of the model and the numerical scheme used in the simulations are described in Appendix B. Although several important mechanisms (such as the constraint release)[1–3] are not considered in this model, we believe that the incorporation of these mechanisms do not change the RF behavior of the TAMSD qualitatively. Therefore, if it gives qualitatively the same result as the slip-spring model, we consider that the RFA can be applied to most of models for entangled polymers.

For simplicity, we employ the discrete version of the tube model. (In the followings we call this model as the discrete reptation model.) As described in Appendix B, we model the tube as a freely jointed chain type model. A tube consists of  $Z$  tube segments and each tube segment has a fixed length  $a$ . (The number of segments in a tube is fixed to be constant and thus the contour length fluctuation (CLF)[1] is absent in this model.) The polymer chain inside the tube moves (reptates) forth or back randomly, and we express the characteristic time scale of this random motion as  $\tau_l \equiv \zeta_l a^2/k_B T$  ( $\zeta_l$  is the friction coefficient of a segment in the longitudinal direction along a tube). We use  $a$  and  $\tau_l$  as elementary length and time scales. The time evolution of a tube is modeled as a random jump type process.

The chain inside the tube reptates forth or back by a given jump rate, and then a segment at an end is destructed and a new segment is constructed at another end. We perform kinetic Monte Carlo simulations for various different values of  $Z$ . ( $Z$  is proportional to the number of chain segments  $N$ .) The number of polymer chains (or tubes) is 1024 for each simulation, and the initial state is sampled from an equilibrium distribution. Because this model lacks the CLF mechanism, the MSD of the CM becomes the following form[23], instead of Eq. (2):

$$\langle [\mathbf{r}_{\text{CM}}(t) - \mathbf{r}_{\text{CM}}(0)]^2 \rangle \propto t. \quad (6)$$

The EAMSDs of CMs are shown in Fig. 4. All EAMSDs are proportional to  $t$  in all the time regions, which is consistent with Eq. (6). Therefore, in the discrete reptation model, we cannot obtain any characteristic time scales from the EAMSD at all.

Interestingly, even in this case, the RF of the TAMSDs shows a clear crossover. As in the case of the slip-spring model, an appropriate value should be chosen for  $\Delta$  in the RFA. Here we set  $\Delta/\tau_l = 10$ . (We show the effect of  $\Delta$  value in Appendix A.) As shown in Fig. 5, the RF is fitted well with Eq. (5). Unlike the case of the slip-spring model, the exponent  $\alpha$  is almost zero, which is different from the results of the slip-spring model. Moreover, we observe that the crossover time strongly depends on  $Z$  in a similar way to the case of the slip-spring model. The crossover time  $\tau_c$  obtained from the RF of the TAMSDs are shown in Fig. 6. The obtained  $\tau_c$  data almost coincide with the longest relaxation time  $\tau_d$  or the reptation time  $\tau_{\text{rep}} = \tau_l Z^3/\pi^2$ . This becomes clearer if we rescale the time  $t$  by the reptation time  $\tau_{\text{rep}}$ . Figure 7 shows the RFs of TAMSDs (the same data as Figure 5) for the rescaled time  $t/\tau_{\text{rep}}$ . Interestingly, the rescaled RF data for different  $Z$  collapse into one master curve if  $Z$  is sufficiently large, except the short time region.

### III. DISCUSSIONS

Both the slip-spring model and the discrete reptation model in Section II give qualitatively the same crossover behavior. However, there are some differences between the RFA results of the slip-spring and discrete reptation models. For example, the slip-spring model exhibits the power-law type behavior of  $R(t; \Delta)$  for  $t \lesssim \tau_c$  while the discrete reptation model exhibits almost constant  $R(t; \Delta)$  for  $t \lesssim \tau_c$ . We expect that the differences reflect the detailed relaxation mechanisms of models. (In the case of the CTRW,  $R(t; \Delta)$  reflects some informations of traps[16].)

The discrete reptation model is the simple model and the reptation is only the relaxation mechanism in the model. On the other hand, the slip-spring model has other relaxation mechanisms such as the Rouse motion of subchains and the contour length fluctuation. The incorporation of additional relaxation mechanisms other than the reptation modulates several dynamical behavior[1–3, 24]. In the reptation model, the dynamic equation of the CM is described by using the end-to-end vector[23]. Thus the RFs can be also modulated by various relaxation mechanisms, for example, through the dynamics of the end-to-end vector. If our expectation is correct, we will be able to extract the information about the relaxation mechanisms from the RFA. However, currently we have no analytical theory for the RFs in entangled polymer systems. Unfortunately, it seems to be difficult to obtain analytical expressions of RFAs of CMs, and the development of theoretical tools for RFs is desired.

Although we have examined only two models and some mechanisms are not considered in them, we believe that we will observe similar behavior of TAMSDs for other models of entangled polymers. Judging from our simulation data, the reptation motion is the most important for the behavior of the RFs. Therefore, even if various mechanisms which affect the relaxation behavior are incorporated, we expect that the RFA still gives the information about the long time relaxation due to the reptation. It should be pointed that several mechanisms such as the CR affect the longest relaxation time  $\tau_d$ [2, 3, 24]. We expect that the crossover time  $\tau_c$  will be affected in a similar way, and thus the RFA will give qualitatively the same results for more elaborated models. The numerical factor would be largely affected by mechanisms such as the CLF and the CR. The discrepancy between  $\tau_d$  and  $\tau_c$  observed in the slip-spring model may be due to such additional relaxation mechanisms. From these considerations, we expect that the RFA performed in Section II can be applied for other models, including the Kremer-Grest model[4] or highly coarse-grained models[7, 8].

Here we shortly discuss the power-law exponent  $\alpha$  of the slip-spring model (Eq. (5)). As we have shown in Section IIA, it depends on  $N$ . As far as the authors know, there is no relaxation mechanism which gives such  $N$ -dependent power-law exponent. Therefore, it would be physically natural to interpret that this  $N$ -dependent power-law exponent is apparent. As we can observe in Fig. 2(b), the RF becomes proportional to  $t^{-0.5}$  for a very small  $t$  region. The region where we have observed the power-law exponent  $\alpha$  is the transient region. If  $N$  is relatively small, such a transient region is affected by the short time region, and the fitting may give apparent power-law exponent which is different from the true value. (This situation may be somewhat similar to the power-law for the longest relaxation time,  $\tau_d \propto N^{3.4}$ , which is considered to be apparent behavior[1].)

One advantage of the RFA is that it can be performed only with the CM trajectory data. As we mentioned, for some cases, the CM trajectory data are more suitable for the calculation of the long time relaxation behavior. The accurate

computation of the stress autocorrelation functions in multi chain models is not easy. In highly coarse-grained models (such as the RaPiD model), the entangled polymers are modeled with very limited degrees of freedom, and some information such as the end-to-end vectors cannot be calculated. The RFA can be applied even for such cases. Of course, the RFA will not always be the optimal method, and other methods which utilize conventional quantities will be better for some cases. The RFA of the CM trajectories should be understood as a complementary method to conventional ones. Here we note that in conventional methods to determine the longest relaxation time  $\tau_d$ , dynamical quantities are utilized after the ensemble averages are taken. On the other hand, the RFA of the TAMSDs uses the time-averaged quantity before the ensemble average is taken. The RFA for other quantities, which are usually analyzed after the ensemble averages are taken, may be possible.

Another advantage of the RFA will be that we can utilize it to validate some phenomenological coarse-grained models. As we will discuss in the next subsection, there are many possible ways to model the dynamics of entangled polymers. The RF behavior of TAMSDs will be useful to check the validity of a phenomenologically constructed dynamical model. That is, if the target model reasonably reproduces the dynamics of entangled polymers, it should exhibit the crossover behavior and the crossover time  $\tau_c$  should be comparable to the longest relaxation time  $\tau_d$  (estimated from other physical quantities). For such a validation, usually the ensemble-averaged quantities (such as the relaxation modulus) are utilized. We expect that the RFA, which utilizes a time-averaged quantity, may become a complementary validation tool.

#### IV. CONCLUSIONS

In this work we have shown evidences that the RFA of the TAMSDs of CMs of polymer chains can be utilized to study the long time relaxation behavior of entangled polymer systems. The information of the longest relaxation time (the disengagement time)  $\tau_d$  is successfully extracted as the crossover time  $\tau_c$  in the RF of the CM trajectories.

The RFA can extract the characteristic long time relaxation behavior of entangled polymers for two different models (the slip-spring model and the discrete reptation model), although the behavior somewhat depends on the model details or parameters. For the discrete reptation model, the crossover time determined from the RF of the TAMSDs almost coincide with the longest relaxation time determined from the shear relaxation modulus.

Although in this work we provided results only for two models, we believe that our method can be applied for other models of entangled polymers, including molecular dynamics models and highly coarse-grained models. Further analyses for various simulation data and development of theories for RFs in entangled polymer systems are demanding.

#### Acknowledgment

This work is supported by the Core Research for the Evolution Science and Technology (CREST) of the Japan Science and Technology Agency (JST).

#### Appendix A: Effect of Time Difference $\Delta$

In this appendix, we examine the effect of the time difference size  $\Delta$  on the RF of the TAMSDs,  $R(t; \Delta)$ . Figure 8 shows the RF for  $N = 80$  and different  $\Delta$  values in the slip-spring model. The forms of  $R(t; \Delta)$  data depend on  $\Delta$  rather strongly. If  $\Delta$  is too large (such as  $\Delta/\tau_0 = 1000$ ), we cannot determine the crossover time  $\tau_c$  from the RF data. This may be because the  $\Delta$  value becomes close to  $\tau_d$  and the crossover behavior may be smeared out. If  $\Delta$  is too small (such as  $\Delta/\tau_0 = 1$ ), the  $R(t; \Delta)$  value becomes very small and thus it becomes difficult to determine  $\tau_c$  accurately. Thus  $\Delta$  is required to be an intermediate value. In this case, the curve for  $\Delta/\tau_0 = 10$  seems to be better than other curves. For other  $N$  cases, we observe a similar trend. Therefore, in this work we employ  $\Delta/\tau_0 = 10$  to determine the crossover time  $\tau_c$ . Physically, this value is comparable to the entanglement time  $\tau_e$ . (We note that even if we employ other value for  $\Delta$ , for example  $\Delta/\tau_0 = 100$ , the result in the main text is qualitatively not affected.)

Figure 9 shows the RF for  $Z = 40$  and several different  $\Delta$  values in the discrete reptation model. As clearly observed in Fig. 9, the  $R(t; \Delta)$  data for relatively small  $\Delta$  ( $\Delta/\tau_l \lesssim 10$ ) are almost the same. Thus we consider that there is a threshold for  $\Delta/\tau_l$  and if  $\Delta$  is smaller than the threshold,  $R(t; \Delta)$  is insensitive to  $\Delta$ . The threshold value depends on several parameters such as  $Z$ . To determine the crossover time  $\tau_c$  for different  $Z$  values, we should choose  $\Delta$  smaller than the threshold for all the  $Z$  values examined. In this work, we employ  $\Delta/\tau_l = 10$ , which is sufficiently small for all the examined parameters in the main text. In this case,  $\tau_l$  is comparable to  $\tau_e$  and thus this  $\Delta$  is slightly larger than  $\tau_e$ .

In conclusion, the results in the main text are not so sensitive to the values of  $\Delta$ , as long as  $\Delta$  is selected to be an intermediate value. Results in this appendix implies that the  $\Delta$  value should be selected comparable to (or slightly larger than) the entanglement time  $\tau_e$ . Although the reason why such  $\Delta$  values work well is not clear, this may be useful to estimate the optimal value of  $\Delta$  when one performs the RFA for other simulation results. A qualitatively similar result is obtained by a theoretical analysis for the CTRW[16].

### Appendix B: Discrete Reptation Model

In this appendix, we provide the details of the discrete reptation model and the numerical scheme used for simulations. In the Doi-Edwards type reptation model[1], the polymer chain is assumed to be confined in a tube which consists of  $Z$  discrete steps. Each step has a constant size  $a$ , and thus the tube can be regarded as a freely jointed chain like object[1]. In this work we express the positions of tube ends and kinks by  $\{\mathbf{R}_i\}$  ( $i = 0, 1, 2, \dots, Z$ ). The chain inside the tube can move only to the direction along the tube (which we call the longitudinal direction), and this reptation motion is modeled by the Langevin equation. However, the Langevin equation is not suitable to describe the dynamics of discrete objects, especially when we perform numerical simulations. In this work, we employ the discrete jump dynamics to model the reptation motion.

In the discretized reptation model, the polymer chain can move forth or back along the chain by the constant segment size  $a$  with one step. We ignore the contour length fluctuation (CLF) effect and the constraint release (CR) effect. Thus the dynamics of the chain is described only by the reptation motion described here. The jump rates are proportional to  $Z^{-1}$ , because the jump rate corresponds to the longitudinal motion of a whole chain along the tube and the effective friction coefficient of a chain is proportional to  $Z^{-1}$ . The forth or back jump rates (transition rates) are given as

$$W_{\pm} = \frac{1}{Z\tau_l} \quad (\text{B1})$$

where  $\tau_l$  is the characteristic longitudinal diffusion time defined as  $\tau_l \equiv \zeta_l a^2 / k_B T$  ( $\zeta_l$  is the friction coefficient of a segment in the longitudinal direction). Subscripts “+” and “-” represents the forth and back directions, respectively. This transition rate model successfully reproduces the diffusion coefficient of a chain along the tube (in the longitudinal direction),  $D_l = k_B T / Z \zeta_l$ [23].

To avoid ambiguities or problems associated with the dynamical mapping of Monte Carlo simulations[25, 26], we employ the kinetic Monte Carlo scheme[26–28] which can handle the time evolution of discrete stochastic jump processes exactly. We start from the equilibrium tube conformation  $\{\mathbf{R}_i\}$  at  $t = t_0$ . To generate random numbers, we employ the Mersenne twister pseudo random number generator[29]. The kinetic Monte Carlo scheme evolves the system from time  $t = t_j$  to  $t = t_{j+1}$  where  $j$  is the number of Monte Carlo steps. We need the total transition rate  $W_{\text{tot}}$  and the (normalized) probabilities of transitions  $P_{\pm}$ , to simulate the time evolution. They are given as

$$W_{\text{tot}} = W_+ + W_- = \frac{2}{Z\tau_l}, \quad (\text{B2})$$

$$P_{\pm} = \frac{W_{\pm}}{W_{\text{tot}}} = \frac{1}{2}. \quad (\text{B3})$$

The direction (forth or back) is randomly selected according to the probability  $P_{\pm}$ . From Eq. (B3) the direction is selected with the same probability, and this can be easily realized by using a uniformly distributed random number. The time step size is sampled from the exponential distribution. The time at the  $(j + 1)$ -th step becomes

$$t_{j+1} = t_j - \frac{1}{W_{\text{tot}}} \ln u \quad (\text{B4})$$

where  $u$  is the random number sampled from the uniform distribution in  $(0, 1)$ . The positions of tube ends and kinks at the  $(j + 1)$ -th step are given as

$$\mathbf{R}_i(t_{j+1}) = \begin{cases} \mathbf{R}_{i+1}(t_j) & (i < Z) \\ \mathbf{R}_Z(t_j) + \mathbf{a}\mathbf{n} & (i = Z) \end{cases} \quad \text{or} \quad \begin{cases} \mathbf{R}_0(t_j) + \mathbf{a}\mathbf{n} & (i = 0) \\ \mathbf{R}_{i-1}(t_j) & (i > 0) \end{cases} \quad (\text{B5})$$

where  $\mathbf{n}$  is the random vector on the three dimensional unit sphere ( $|\mathbf{n}| = 1$ ). The time series of the tube conformation are obtained by successively iterating the kinetic Monte Carlo time steps.

The segments of the polymer chain are assumed to be uniformly distributed along the tube. Then the CM position is calculated from  $\{\mathbf{R}_i\}$  as

$$\mathbf{r}_{\text{CM}} = \frac{1}{Z} \sum_{i=0}^{Z-1} \frac{\mathbf{R}_i + \mathbf{R}_{i+1}}{2}. \quad (\text{B6})$$

For the discrete reptation model, we define the longest relaxation time  $\tau_d$  by using the shear relaxation modulus  $G(t)$  at the long time limit,

$$-\frac{1}{t} \ln \frac{G(t)}{G(0)} \rightarrow \frac{1}{\tau_d} \quad (t \rightarrow \infty). \quad (\text{B7})$$

(This method to determine  $\tau_d$  is consistent with one used for the slip-spring model.) We calculate the shear relaxation modulus by the linear response formula:

$$G(t) = c_0 k_B T \langle \sigma_{xy}(t) \sigma_{xy}(0) \rangle. \quad (\text{B8})$$

Here  $c_0$  is the spatial average chain number density and  $\sigma_{xy}$  is the  $xy$  component of the stress tensor. The stress tensor  $\boldsymbol{\sigma}$  is calculated as

$$\boldsymbol{\sigma} = \frac{3k_B T}{a^2} \sum_{i=0}^{Z-1} (\mathbf{R}_{i+1} - \mathbf{R}_i)(\mathbf{R}_{i+1} - \mathbf{R}_i) - (Z+1)k_B T \mathbf{1}. \quad (\text{B9})$$

We note that Eqs. (B7)-(B9) give the shear relaxation modulus which is proportional to the tube surviving probability[1]. Therefore it is almost obvious for our model that the longest relaxation time  $\tau_d$  coincides to the reptation time  $\tau_{\text{rep}} = \zeta_l Z^3 a^2 / \pi^2 k_B T = Z^3 \tau_l / \pi^2$ .

- 
- [1] M. Doi and S. F. Edwards, *The Theory of Polymer Dynamics* (Clarendon Press, 1986).  
[2] H. Watanabe, Prog. Polym. Sci. **24**, 1253 (1999).  
[3] T. C. B. McLeish, Adv. Phys. **51**, 1379 (2002).  
[4] K. Kremer and G. S. Grest, J. Chem. Phys. **92**, 5057 (1990).  
[5] M. Pütz, K. Kremer, and G. S. Grest, Europhys. Lett. **49**, 735 (2000).  
[6] S. K. Sukumaran and A. E. Likhtman, Macromolecules **42**, 4300 (2009).  
[7] P. Kindt and W. J. Briels, J. Chem. Phys. **127**, 124901 (2007).  
[8] J. T. Padding and W. J. Briels, J. Phys.: Cond. Matt. **23**, 233101 (2011).  
[9] F. Bardou, J. P. Bouchaud, A. Aspect, and C. Cohen-Tannoudji, *Lévy Statistics and Laser Cooling: How Rare Events Bring Atoms to Rest* (Cambridge University Press, 2002).  
[10] R. Metzler and J. Klafter, Phys. Rep. **339**, 1 (2000).  
[11] Y. He, S. Burov, R. Metzler, and E. Barkai, Phys. Rev. Lett. **101**, 058101 (2008).  
[12] J.-H. Jeon and R. Metzler, J. Phys. A: Math. Theor. **43**, 252001 (2010).  
[13] T. Akimoto, E. Yamamoto, K. Yasuoka, Y. Hirano, and M. Yasui, Phys. Rev. Lett. **107**, 178103 (2011).  
[14] T. Miyaguchi and T. Akimoto, Phys. Rev. E **83**, 031926 (2011).  
[15] T. Miyaguchi and T. Akimoto, Phys. Rev. E **83**, 062101 (2011).  
[16] T. Akimoto and T. Miyaguchi, in preparation.  
[17] C. C. Hua and J. D. Schieber, J. Chem. Phys. **109**, 10018 (1998).  
[18] Y. Masubuchi, J. Takimoto, K. Koyama, G. Ianniruberto, F. Greco, and G. Marrucci, J. Chem. Phys. **115**, 4387 (2001).  
[19] M. Doi and J. Takimoto, Phil. Trans. R. Soc. Lond. A **361**, 641 (2003).  
[20] D. M. Nair and J. D. Schieber, Macromolecules **39**, 3386 (2006).  
[21] A. E. Likhtman, Macromolecules **38**, 6128 (2005).  
[22] T. Uneyama, Nihon Reoroji Gakkaishi (J. Soc. Rheol. Jpn.) **39**, 135 (2011).  
[23] M. Doi and S. F. Edwards, J. Chem. Soc. Faraday Trans. 2 **74**, 1789 (1978).  
[24] A. E. Likhtman and T. C. B. McLeish, Macromolecules **35**, 6332 (2002).  
[25] K. Binder and D. W. Heermann, *Monte Carlo Simulation in Statistical Physics: An Introduction*, 4th ed. (Springer, Berlin, 1997).  
[26] A. Chatterjee and D. G. Vlachos, J. Computer-Aided Mater. Des. **14**, 253 (2007).  
[27] D. T. Gillespie, J. Comp. Phys. **22**, 403 (1976).  
[28] D. T. Gillespie, Annu. Rev. Phys. Chem. **58**, 35 (2007).  
[29] M. Matsumoto and T. Nishimura, ACM Trans. Model. Comp. Simul. **8**, 3 (1998), <http://www.math.sci.hiroshima-u.ac.jp/~m-mat/MT/emt.html>.

### Figure Captions

Figure 1: Ensemble-averaged EAMSDs of CMs in the slip-spring model for  $N = 10, 20, 40, 80$ , and  $160$ . Dashed lines represent curves which are proportional to  $\Delta^1$  and  $\Delta^{1/2}$ .  $b$  and  $\tau_0$  are the size and characteristic time of a segment, respectively.

Figure 2: Relative fluctuations of TAMSDs of CMs in the slip-spring model for  $\Delta/\tau_0 = 10$  and  $N = 10, 20, 40, 80$  and  $160$ , where  $\tau_0$  is the characteristic time of a segment. (a)  $N = 10$  and  $20$ , and (b)  $N = 40, 80$ , and  $160$ . Dashed line represents a curve proportional to  $t^{-1/2}$ . The power law exponents for the short time regions are  $\alpha = 0.31, 0.24$ , and  $0.19$  for  $N = 40, 80$ , and  $160$ , respectively.

Figure 3: The longest relaxation time  $\tau_d$  and the crossover time  $\tau_c$  in the slip-spring model.  $\tau_d$  is determined from the shear relaxation modulus data [22] whereas  $\tau_c$  is determined from the RF data of TAMSDs for  $\Delta/\tau_0 = 10$ . Dashed lines represent fitting curves for large  $N$  ( $\tau_d \propto N^{3.48}$  and  $\tau_c \propto N^{3.51}$ ).

Figure 4: Ensemble-averaged MSDs of CMs in the discrete reptation model for  $Z = 10, 20, 40, 80$ , and  $160$ .  $a$  is the step size of a tube segment and  $\tau_l$  is the characteristic time of the longitudinal motion of a segment along the tube.

Figure 5: Relative fluctuations of TAMSDs of CMs in the discrete reptation model for  $\Delta/\tau_l = 10$  (see Appendix A) and  $Z = 10, 20, 40, 80$  and  $160$ . The dashed line represents a curve proportional to  $t^{-1/2}$ .  $\tau_l$  is the characteristic time of the longitudinal motion of a segment along the tube.

Figure 6: The longest relaxation time  $\tau_d$  and crossover time  $\tau_c$  in the discrete reptation model.  $\tau_d$  is determined from the shear relaxation modulus and  $\tau_c$  is determined from the RF data of TAMSDs in the same way of Fig. 3. The dashed line represents the reptation time  $\tau_{\text{rep}}/\tau_l = Z^3/\pi^2$ .

Figure 7: Rescaled RFs of TAMSDs of CMs in the discrete reptation model for different values of  $Z$ . The data are the same as Figure 5 but the observation time  $t$  is rescaled by the reptation time  $\tau_{\text{rep}} = Z^3\tau_l/\pi^2$ . All the data points collapse into one master curve except the short time region or the small  $Z$  data ( $Z = 10$ , in this case).

Figure 8: Relative fluctuations of TAMSDs of CMs in the slip-spring model for  $N = 80$ . The dashed line represents a curve proportional to  $t^{-1/2}$ .

Figure 9: Relative fluctuations of TAMSDs of CMs in the discrete reptation model for  $Z = 40$ . The dashed line represents a curve proportional to  $t^{-1/2}$ .



## Figures

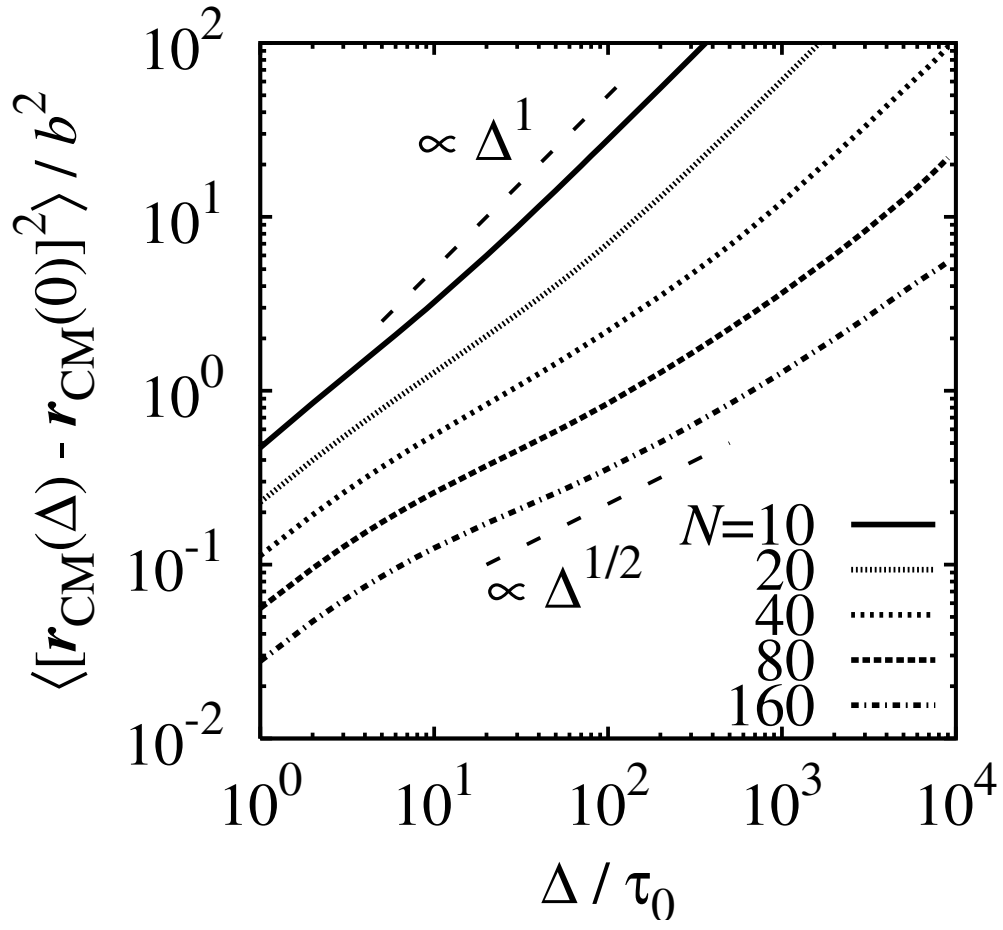


FIG. 1:

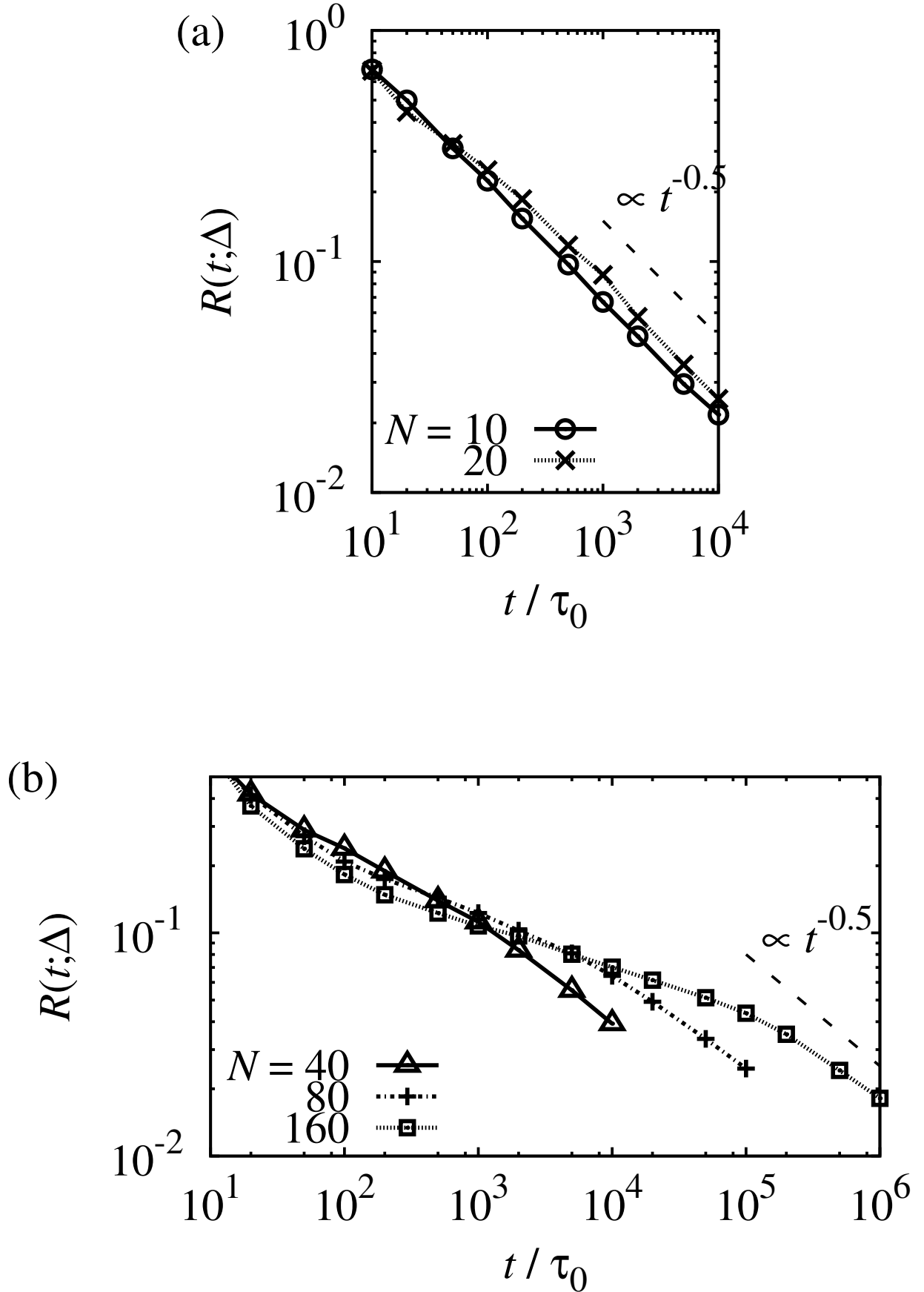


FIG. 2:

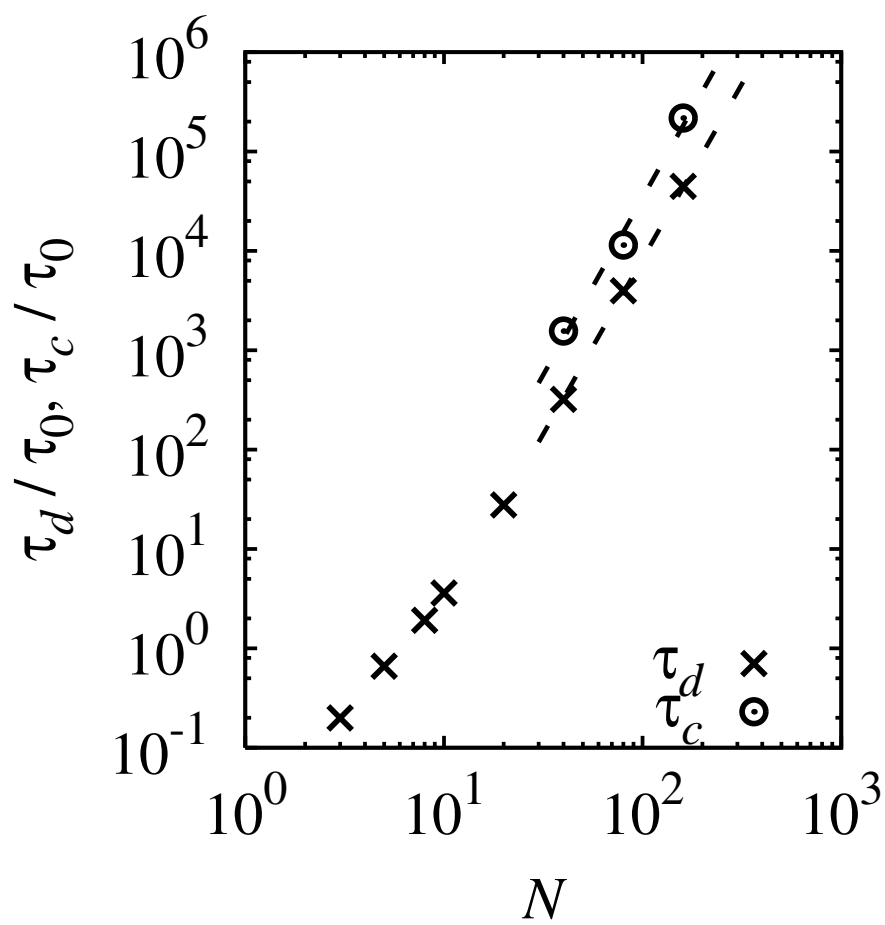


FIG. 3:

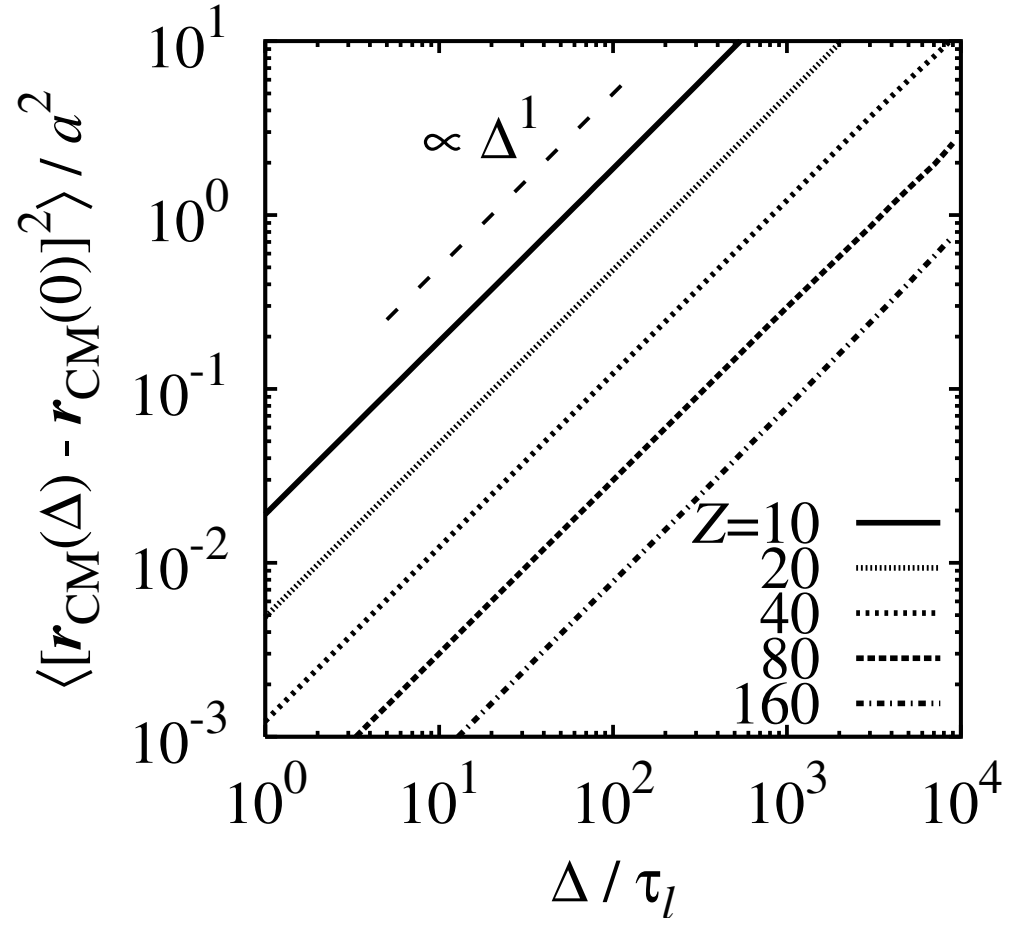


FIG. 4:

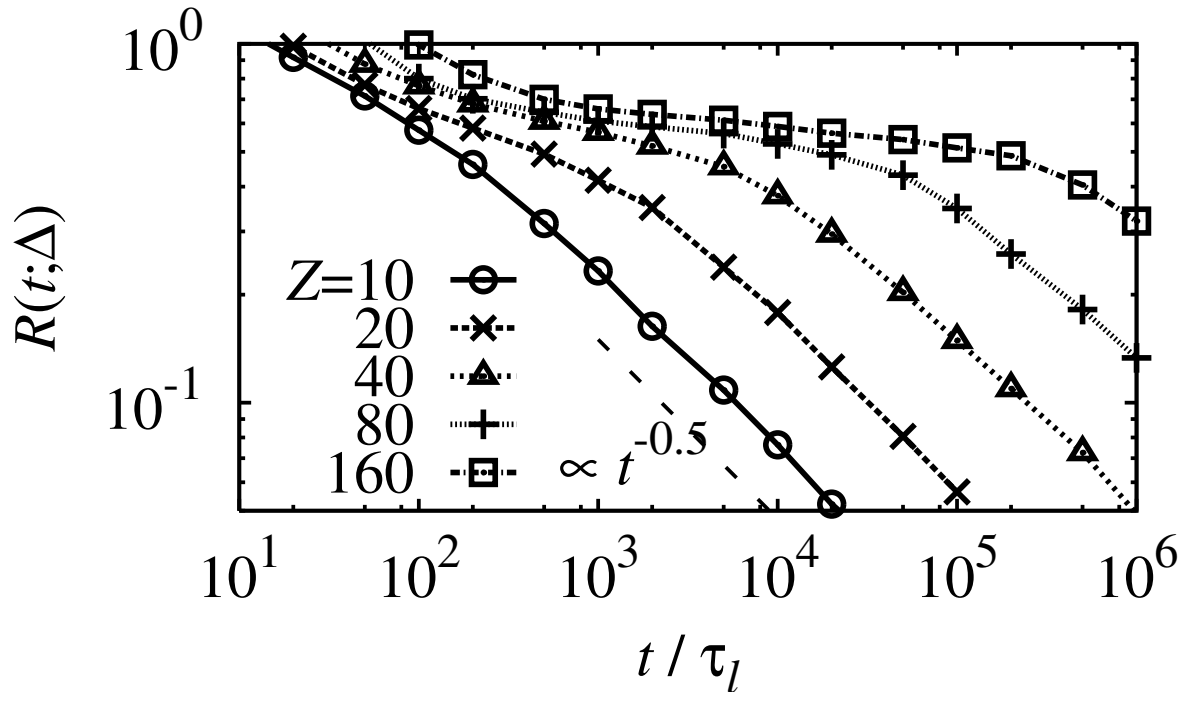


FIG. 5:

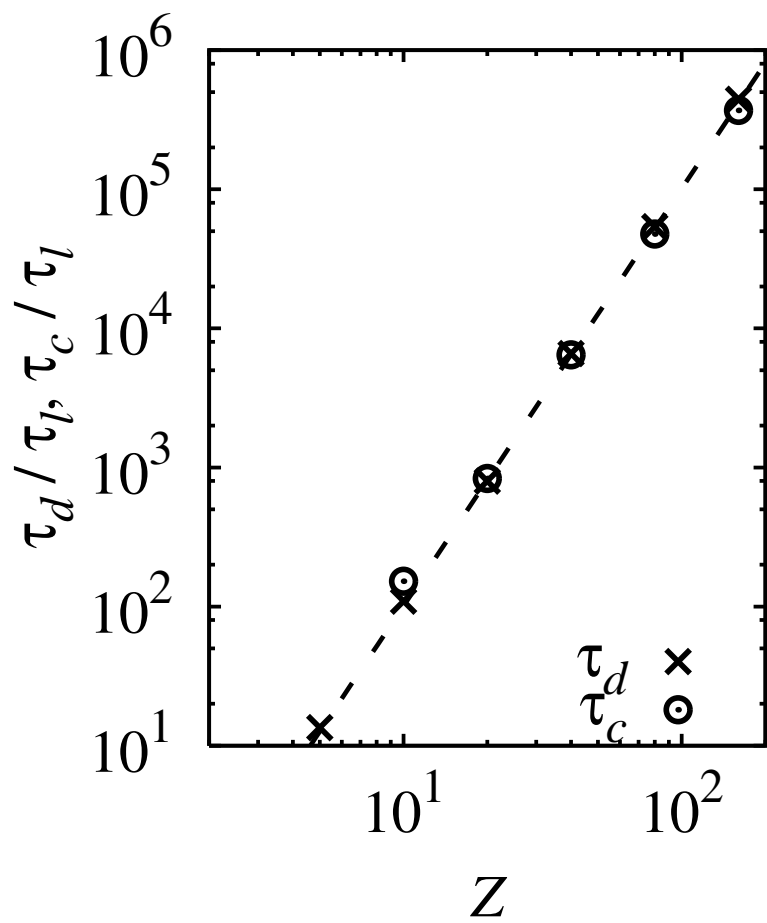


FIG. 6:

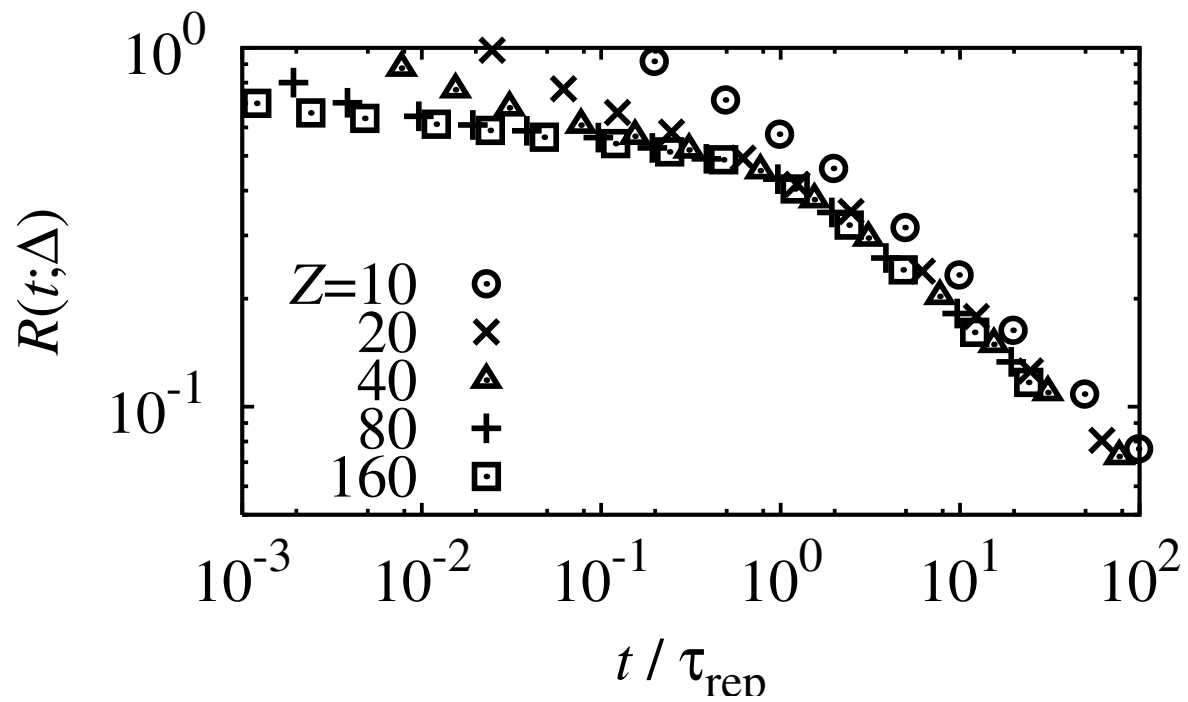


FIG. 7:

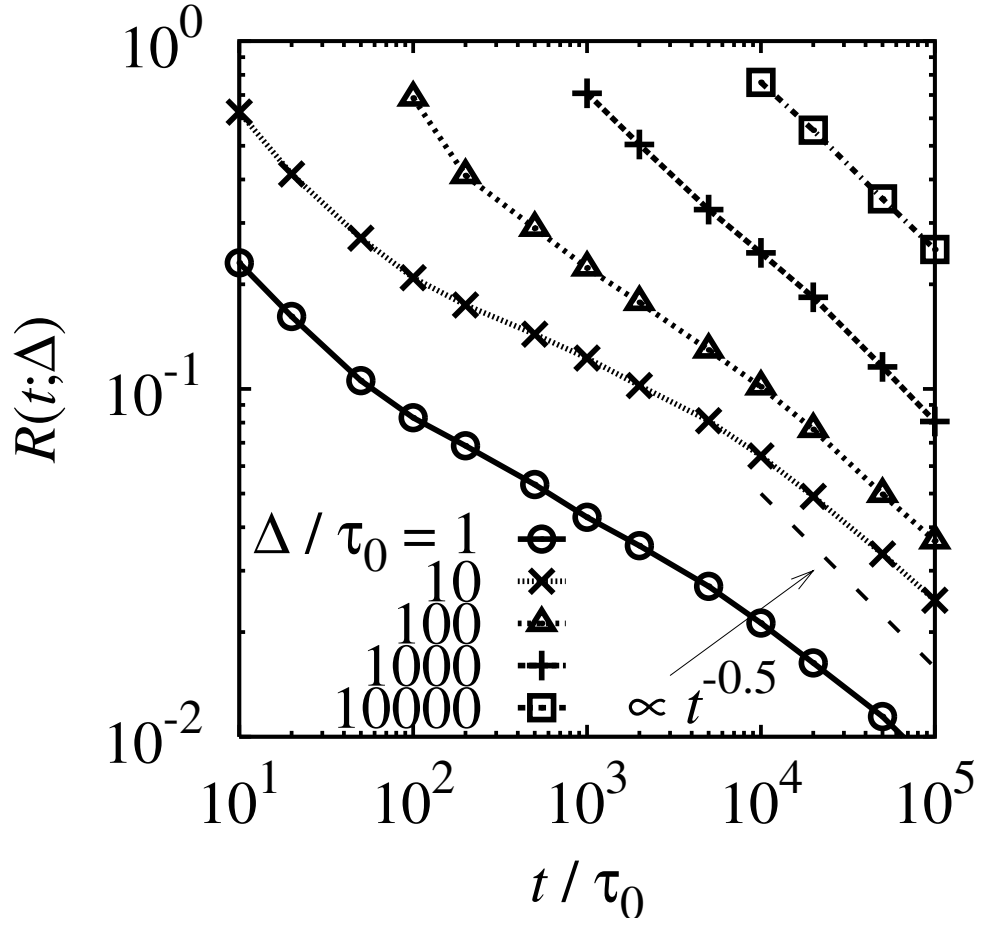


FIG. 8:



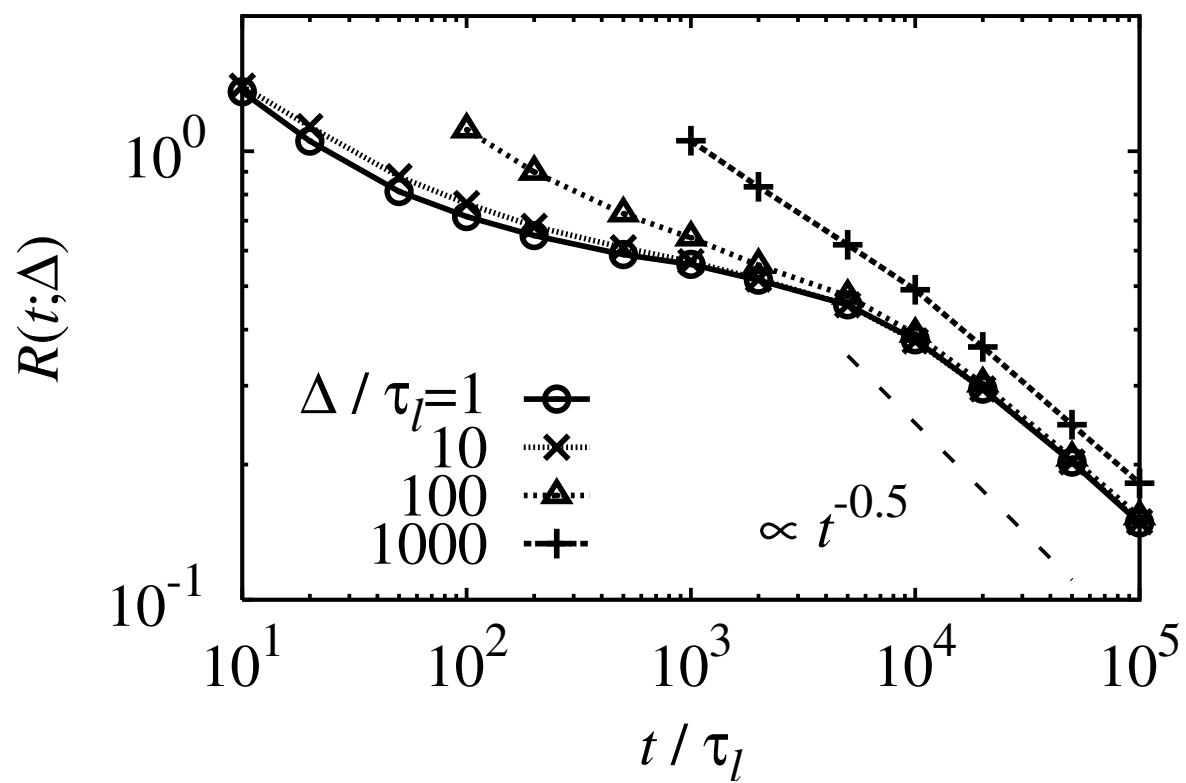


FIG. 9: